Spontaneous emission rate of an electric dipole in a general microcavity

Jeong-Ki Hwang, Han-Youl Ryu, and Yong-Hee Lee
Department of Physics, Korea Advanced Institute of Science and Technology, Taejon 305-701, Korea
(Received 24 February 1999)

A simple method to obtain the spontaneous emission rate of a dipole placed in a general microcavity is proposed and demonstrated. In our approach, Maxwell's equations are solved directly in real space instead of *k* space by the finite-difference time-domain method with a free-space boundary condition. It is advantageous that allowed eigenmodes need not be calculated and the total radiation rates to all the allowed modes are obtained from the beginning. All the localized modes, guided modes, and extended modes are inherently included in this formulation. The validity of the method is tested for a dipole placed in an ideal planar microcavity and the calculated results agree well with the closed-form analytic solutions. The enhancement and the inhibition of the spontaneous emission rate in several photonic band-gap structures are studied. Point dipole analyses show three-dimensional effects in two-dimensional in-plane photonic band gaps and the effects of localized, guided and extended modes on radiation rates. [S0163-1829(99)03931-4]

I. INTRODUCTION

In 1946 Purcell[1] predicted that the probability of spontaneous emission could be altered by the existence of different electromagnetic mode distributions from the mode distributions of free space. Since then marked progress has been achieved in controlling spontaneous emission with the use of wavelength-sized cavities. This research field is now called cavity quantum electrodynamics.[2,3] Prominent examples of these microcavities can be made with photonic crystals,[4–6] where spontaneous emission can be enhanced, attenuated, or even suppressed by changing the density of electromagnetic states or the orbital angular momentum of the emitted photon.[7] The ability to control spontaneous emission can have profound consequences on many opto-electronics devices.[8–10] Several investigators have tried to calculate how spontaneous emission changes with more realistic optical microcavity structures made by dielectric materials.[11–17,20] However, further progress in the theoretical work is needed for a better understanding of the real world microcavities.

The spontaneous emission enhancement factor of an excited atom in a microcavity is estimated roughly for a localized resonant mode by the ratio of the density of electromagnetic modes available for the emitted photon to the density of free-photon states $Q/8\pi(\Omega/\lambda^3)$, where Q is the quality factor of the cavity, Ω is the effective spacial volume of the resonance, and λ is the wavelength of light.[2] In simple structures, such as a planar microcavity[3,11,12] or a cylindrical waveguide,[2] analytic solutions can be easily found. However, for complex microcavities, such as vertical cavity surface-emitting lasers, proper approximations are assumed to obtain mode profiles.[13] For photonic crystals, the relative changes of the spontaneous lifetime in the photonic crystal were estimated by simply taking the ratio of permitted solid angles in *k* space to the total solid angle 4π.[14] However, this approach is oversimplified. Rigorously, the radiation rate to a specified mode is derived by the use of Maxwell's equations with an electric dipole, a dyadic Green's function, and Poynting theorem.[15] Another group also formulated a Green's-function method to calculate the radiation rate by a dipole to a specified mode.[16] In these two approaches, the spontaneous emission rate for a dipole is represented by the summation of the radiation rate for each allowed mode at a given frequency. The field distributions of all the allowed modes and the dispersion relation are needed. For the dipole in an infinite three-dimensional photonic crystal, allowed modes and the dispersion relation are obtained by use of the plane-wave expansion method and the tetrahedron *k*-space integration.[17] However, these requirements are practically difficult to satisfy in the actual microcavities. So the application range of these approaches in calculating the spontaneous emission rate is limited to simple structures or a specified mode whose eigenfrequency is isolated from the frequencies of other modes.[18–20] Therefore, a more general method applicable to general geometry and frequency distribution is needed.

In this paper we directly solve inhomogeneous Maxwell's equations for general finite microcavities in real space with a finite-difference time-domain method[21] and a perfectly matched layer free-space boundary condition[22] without using the Green's function to calculate spontaneous emission rates. By solving Maxwell's equations in real space instead of *k* space, the summation of the radiation rate to each allowed mode can be avoided for finite microcavities. The spontaneous emission rate—the summation of the radiation rate to all the allowed modes at a given frequency—can be obtained from the beginning. The field distributions of the allowed modes and the dispersion relation are not needed. All the localized modes, guided modes, and extended modes are inherently included in this formalism. This approach can be applied to cavities of arbitrary geometry that contain complex electromagnetic mode distribution.

In Sec. II we briefly describe the method used for the calculation of the radiation rate of spontaneous emission. In Sec. III we applied our formalism to an ideal planar microcavity to test the validity of this approach. Then our method is applied to calculate spontaneous emission in finite dielectric structures with and without a defect in square lattices. Emission characteristics of a point dipole are compared with those of a line dipole. Through this comparison, two-dimensional (2D) and three-dimensional (3D) points of view

 ©1999 The American Physical Society

are discussed. Finite triangular lattice dielectric slabs[9,10] are also analyzed. In Sec. IV we summarize the results.

II. METHOD OF CALCULATION

In our approach the spontaneous emission enhancement factor is the ratio of the radiation rate of a dipole in a microstructure to the radiation rate of a dipole in a homogeneous medium. The radiation rate by a dipole is given by the surface integral of the normal component of the Poynting vector on the closed surface containing the dipole. The Maxwell equations that describe the radiation field of our problem are given by

$$\nabla \cdot \{\epsilon(\mathbf{r})\mathbf{E}(\mathbf{r},t)+\mathbf{P}_d(\mathbf{r},t)\}=0, \tag{1}$$

$$\nabla \cdot \mathbf{H}(\mathbf{r},t)=0, \tag{2}$$

$$\nabla \times \mathbf{E}(\mathbf{r},t)=-\mu(\mathbf{r})\frac{\partial}{\partial t}\mathbf{H}(\mathbf{r},t), \tag{3}$$

$$\nabla \times \mathbf{H}(\mathbf{r},t)=\frac{\partial}{\partial t}\{\epsilon(\mathbf{r})\mathbf{E}(\mathbf{r},t)+\mathbf{P}_d(\mathbf{r},t)\}. \tag{4}$$

Here $\epsilon(\mathbf{r})$ and $\mu(\mathbf{r})$ are the position-dependent permittivity and permeability, respectively. $\mathbf{P}_d(\mathbf{r},t)$ is the polarization from a dipole source. These equations are solved with the finite-difference time-domain method.[21] To deal with finite microcavities in free space or infinite but not periodic microcavities we use the perfectly matched layer (PML) boundary condition.[22] This boundary condition faithfully simulates infinite space filled with the same materials as the materials near the boundary. Therefore, this PML condition is useful to represent finite structures in infinite uniform space or waveguide structures with uniform extension.[23] To obtain the spontaneous emission rate at different frequencies in a single simulation run, Gaussian pulse excitation is analyzed by discrete Fourier transformation.[24] The symmetry of the computational domain is considered to reduce calculation loads. The validation of this classical approach for cavity-induced changes of the spontaneous emission rate that are of a purely quantum electrodynamical origin—a direct consequence of the existence of the vacuum field fluctuations—had been previously argued.[12,15]

III. RESULT AND DISCUSSION

A. Planar microcavity

We begin by applying this approach to a point dipole in a planar microcavity consisting of two infinite-plane perfect conductors. The spontaneous emission rate in this cavity has analytic expression and the enhancement and inhibition are verified in several experiments.[3,11,12,25] The schematic diagram of the setup is shown in Fig. 1(a). The PML encloses the domain, as can be seen from the top side view at the right-hand side. The infinite perfect mirror boundary condition limits the possible value of normal components of wave vector $\mathbf{k}_z$ to $k_z=n\pi/L$, where n is zero or a positive integer and L is the spacing between the mirrors. On the other hand, the magnitude of the parallel component of wave vector $\mathbf{k}_\rho$

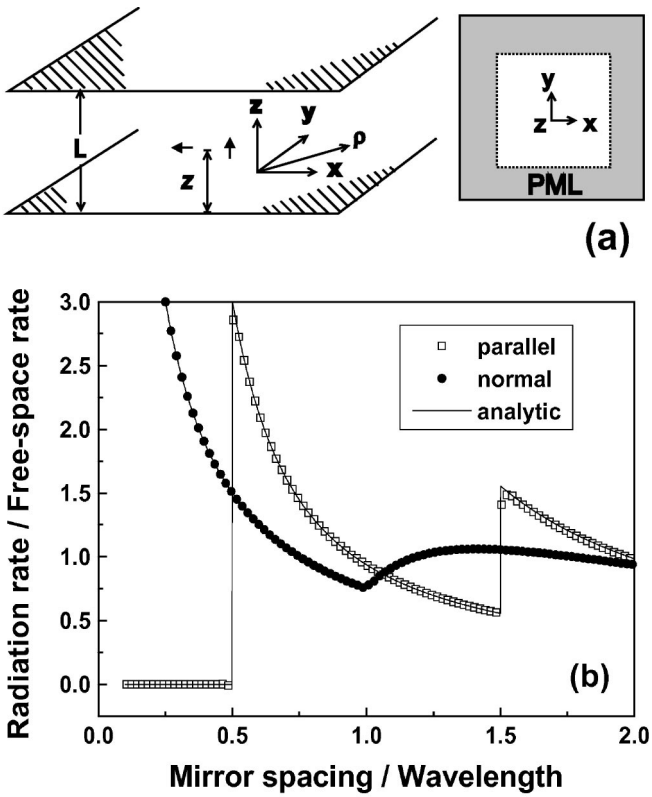

FIG. 1. (a) Schematic diagram of the computational cell of a dipole at a distance z from the bottom plane with a top view of the domain at the right side. (b) Radiation rate of a point dipole at the center of an ideal parallel-plate waveguide relative to the rate in free space. The abscissa is the spacing between the plates relative to the wavelength of the radiation in free space. Boxed dots represent the ratio γ_ρ/γ_o for a point dipole parallel to the plates and circular dots represent the ratio γ_z/γ_o for a point dipole normal to the plates. Lines represent the radiation rates from analytic solutions.

satisfies $\omega^2_{k_z,\mathbf{k}_\rho}=c^2(k_z^2+k_\rho^2)$ and any direction of $\mathbf{k}_\rho$ is possible in plane. The radiation rate for a point dipole normal to the mirrors γ_z is

$$\gamma_z=\gamma_o\left(\frac{3\lambda}{4L}\right)\left\{1+\sum_{n=1}^{[2L/\lambda]}2\left[1-\left(\frac{n\lambda}{2L}\right)^2\right]\cos^2\left(\frac{n\pi z}{L}\right)\right\}, \tag{5}$$

and the radiation rate for a dipole parallel to the mirror γ_ρ is

$$\gamma_\rho=\gamma_o\sum_{n=1}^{[2L/\lambda]}\left[1+\left(\frac{n\lambda}{2L}\right)^2\right]\sin^2\left(\frac{n\pi z}{L}\right) \tag{6}$$

in which $[2L/\lambda]$ indicates the largest integer less than $2L/\lambda$, i.e., the largest allowed value of n. γ_o is the free-space radiation rate and z is a distance from surface of the bottom mirror.

The spontaneous emission enhancement factors γ_z/γ_o and γ_ρ/γ_o for a point dipole at the center of the cavity versus the normalized plate separation L/λ are calculated by our approach and shown with those of analytic solutions presented by solid lines from Eq. (5) and (6) in Fig. 1(b). Note that the field distributions of the allowed modes are not explicitly solved in our calculation. For a point dipole parallel to the mirrors the complete inhibition of radiation when the

spacing is less than $\lambda/2$ and discontinuities each time the spacing is an odd multiple of $\lambda/2$ are shown. For a point dipole perpendicular to the mirrors, the rate has similar discontinuities whenever the spacing is an even multiple of $\lambda/2$. The discontinuities are related to resonances of the cavity. Figure 1(b) shows good agreements between the calculated radiation rates and analytic values. This agreement also demonstrates the performance of the PML in representing infinite free space.

In our calculation of the radiation rates of a point dipole, the infinite planes are represented as finite-size planes enclosed with the PML. The domain is divided into $160\times40\times161$ cells to reduce numerical dispersion at the high-frequency regime.[26] And somewhat thick 20 layers of PML are used to reduce the unwanted reflection at the low-frequency (long wavelength) regime.[27] The half-wavelength-spacing mirror cavity are simulated with the $2\lambda\times0.5\lambda\times2\lambda$ domain and the results agree well with those of the analytic solution for $\infty\times0.5\lambda\times\infty$.

B. Finite square lattice

The 2D photonic band-gap structure based on the square lattice made of circular dielectric rods of infinite length is studied next. Concentrating on the propagation in the plane normal to the rods, the waves can be decoupled into two transversely polarized modes, transverse electric (TE) and transverse magnetic (TM), depending on whether the electric or magnetic field is normal to the rods due to the translational symmetry along their axes.[28] This structure has an in-plane band gap for TM modes, but none for TE modes in the low-frequency region.[6] A line dipole parallel to the rods conserves this translation symmetry and we can expect the complete inhibition of spontaneous emission in the TM in-plane band gap. However, for a point dipole, it is no longer the case. For off-plane propagation the TM band gap does not remain open. At certain propagation angles the band gap becomes closed and a point dipole can radiate through the out-of-plane direction at angles larger than that angle.[29–32] Since we are interested in finite cavities rather than periodic crystals, we choose the system consisting of a finite number of rods. Later, we introduce a defect in this structure to make a microcavity with a resonance mode. It is worth pointing out that all the previous methods experience nontrivial difficulties in handling this kind of finite-size structure with continua of frequency spectra.

The schematic diagram of the setup for $5\times5-1$ is shown in Fig. 2(a). The first 5 indicates five rods along the x axis, the second 5 mean five rods along the y axis, and -1 indicates a single defect at the center of the structure. a and r represent the lattice constant and the radius of the rods, respectively. ϵ_r and ϵ_o denote the permittivity of circular rods and free space, respectively. The size of the structure is assumed to be finite in the x,y plane and infinite along the z axis. PML encloses the structure and simulates this assumption well.[23] For numerical calculation, $r=0.2a$, $\epsilon_r=8.9\epsilon_o$ is used. Figure 2(b) shows the photonic band diagram of the regular square lattice of the circular rods by means of the plane-wave expansion method.[33] A band gap for TM modes is observed between frequencies $0.32c/a$ and $0.44c/a$.

The spontaneous emission enhancement factors are calculated by E_z-polarized line dipoles located at the center of 6

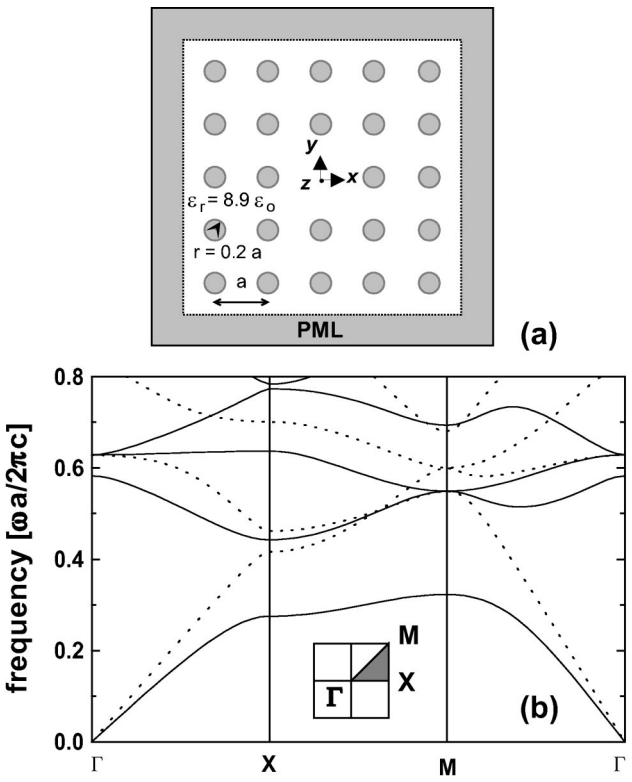

FIG. 2. (a) Schematic diagram of the computational cell for a $5\times5-1$ cavity based on a square lattice. (b) The photonic band diagram for a square array of dielectric columns with $r=0.2a$. A solid line represents TM modes and a dotted line represents TE modes. The inset shows the Brillouin zone, with the irreducible zone shaded light black.

$\times6$ and 7×7 structures in Fig. 3(a). The dipole is located in the air for the 6×6 structure but in a dielectric rod for the 7×7 structure. Comparing with the corresponding photonic band diagram in Fig. 2(b), the spontaneous emission shows very strong inhibition in the TM in-plane band-gap region and enhancement near the band edge. The enhancement of spontaneous emission shows noticeable dependence on the position of the dipole. In fact, the rate at which atoms decay depends on the coupling between the atom and the photon as well as on the density of electromagnetic modes available for the emitted photon. It can also be seen in the analytic expressions of Eqs. (5) and (6) derived for a planar microcavity. However, the inhibition of radiation in the band gap is clearly shown in both cases.

The results of E_z-polarized point dipoles located at the center of 6×6 and 7×7 structures are shown in Fig. 3(b). The inhibition of radiation in the TM in-plane band gap and the enhancement near the band edge are found but not large compared with the results for an E_z-polarized line dipole. This is ascribed to the allowed off-plane propagation.

For an E_y-polarized point dipole, the radiation rates are calculated and shown in Fig. 3(c). The dependence of the radiation rate on the position of the dipole can be observed. In this case, the enhancement and inhibition of the radiation rate related to the band gap is not found and this result is consistent with the nonexistence of the TE in-plane band gap.

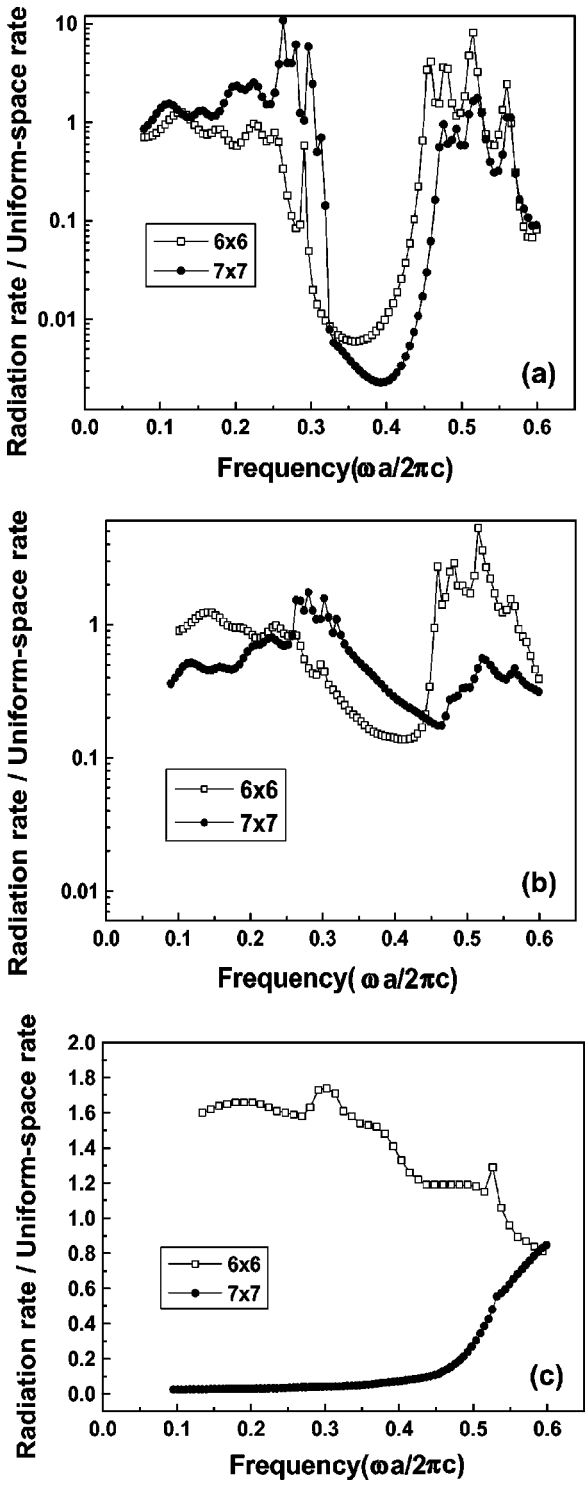

FIG. 3. Radiation rate of a dipole at the center of the 6×6 (dipole in the air) and 7×7 (dipole in the dielectric) structures relative to the rate in uniform space ($\epsilon_r=8.9\epsilon_o$). The TM band gap for the corresponding infinite structure exists between frequencies $0.32c/a$ and $0.44c/a$. (a) A line dipole parallel to the rods. (b) An E_z-polarized point dipole parallel to the rods. (c) An E_y-polarized point dipole normal to the rods.

C. Finite square lattice with a defect

The localized defect mode inside the photonic band gap has been suggested to be useful for the concept of the single-mode light-emitting diode microcavity.[6,8,10] Here 2D photonic lattices with defect modes are selected and studied mainly because of the difficulties in fabricating 3D structures in the optical region. Previously the radiation rate of an E_z-polarized point dipole in a square lattice shows the inhibition of spontaneous emission in the TM in-plane band gap region. Now a defect is introduced in the structure[28,33–35] and the radiation rate of an E_z-polarized point dipole is calculated as shown in Fig. 4(a). For comparison, the result of a line dipole is included as an inset. Significant enhancement of the radiation rate for the point dipole due to the in-plane band gap is observed near the defect-mode frequency. For a line dipole, the enhancement of spontaneous emission is even larger because a defect mode is strongly localized in the band gap. Since no band gap exists for the TE mode the radiation rate for an E_y-polarized point dipole, shown in Fig. 4(b), is not much different from that placed in free space.

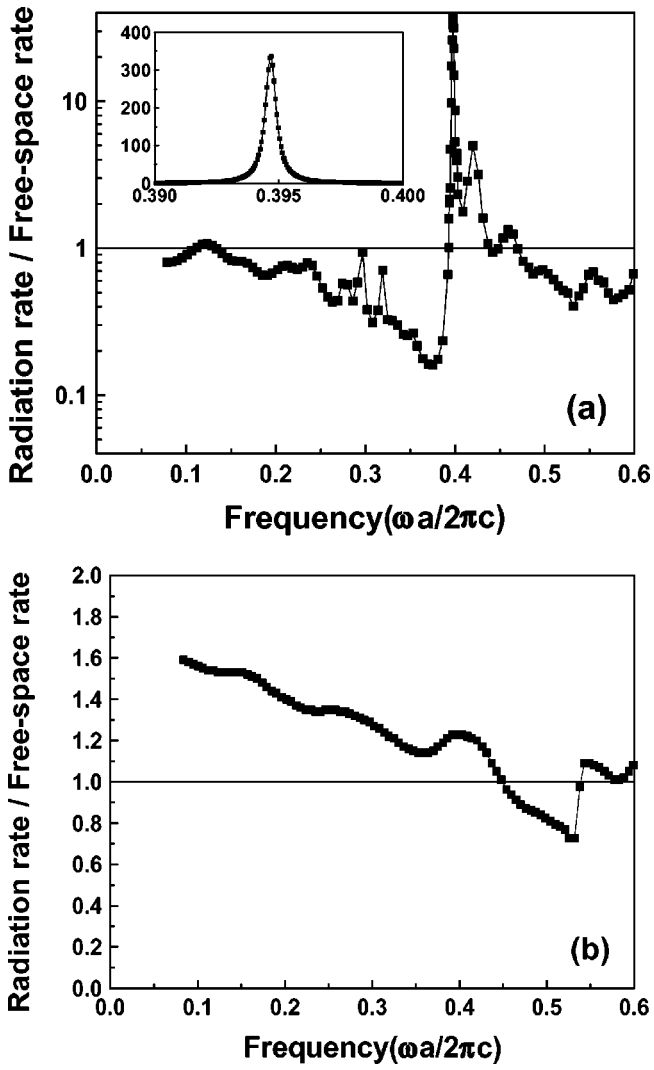

FIG. 4. Radiation rate of a dipole at the center of the defect of the $7\times7-1$ structure. (a) An E_z-polarized point dipole parallel to the rods. The inset shows the radiation rate for a line dipole parallel to the rods. (b) An E_y-polarized point dipole normal to the rods.

D. Finite triangular lattice slab

So far 2D photonic crystals with infinite length are treated. However, in real situations these structures are im-

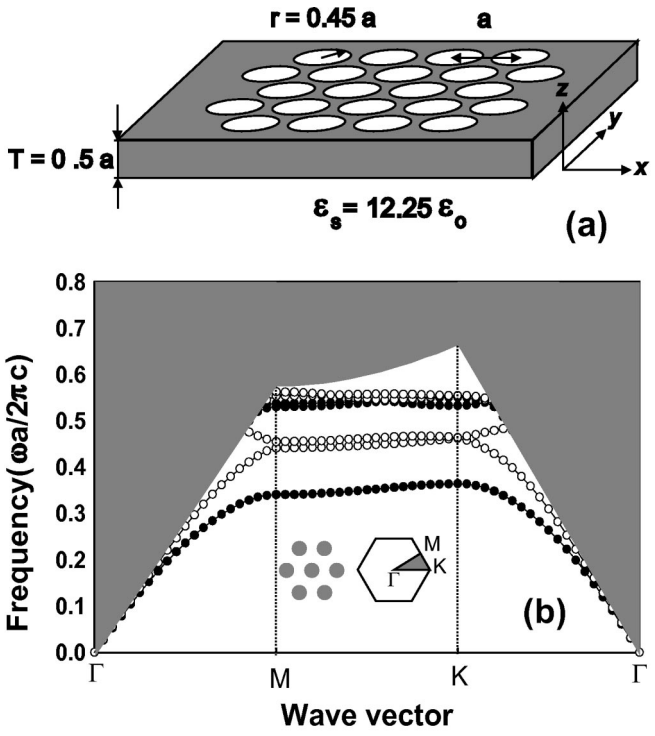

FIG. 5. (a) Schematic diagram of the computational cell containing a finite number of air holes inside a dielectric slab on a triangular lattice. (b) Dispersion relation of the structure shown in (a) for the case of an infinite number of air holes. The gray area corresponds to the continuum of extended modes. The solid circles correspond to TE-like guided modes, while the open circles correspond to TM-like guided modes.

possible to realize. Therefore, 2D slab structures of finite thickness are drawing practical attention. A 2D triangular lattice with circular air holes in an infinite dielectric material is known to have a large in-plane band gap for both TE and TM polarizations.[29] Moreover, the triangular lattice of air holes patterned on the dielectric slab was also reported to have a frequency region without a guided mode. This structure, shown in Fig. 5(a), has been proposed as a high extraction efficiency light-emitting diode by Fan *et al.*[9] In the light-emitting structure that has a large surface, area such as the patterned slab, the total radiative recombination rate and the extraction efficiency need to be considered in addition to the residual nonradiative recombination.

Parameters used for our calculation are the same as Ref. 9. The holes have a diameter of $0.45a$, where a is the lattice constant of the triangular array. The thickness of the slab is $0.5a$ and the permittivity of the slab is $12.25\epsilon_o$. The photonic band diagram for the corresponding slab with an infinite array of holes is plotted in Fig. 5(b). The gray region above the light line corresponds to a continuum of extended modes. The extraction efficiency is defined as the fraction of emitted flux through the top and bottom surfaces of the slab to the total emitted flux.[9] This efficiency is obtained by the ratio of the z component of the Poynting vector integrated over a rectangular parallelepiped to the normal component integrated over the same surface. The height of the parallelepiped is slightly larger than that of the slab and the width and the length is long compared with the height to maximize the collecting angle of the extracted light.

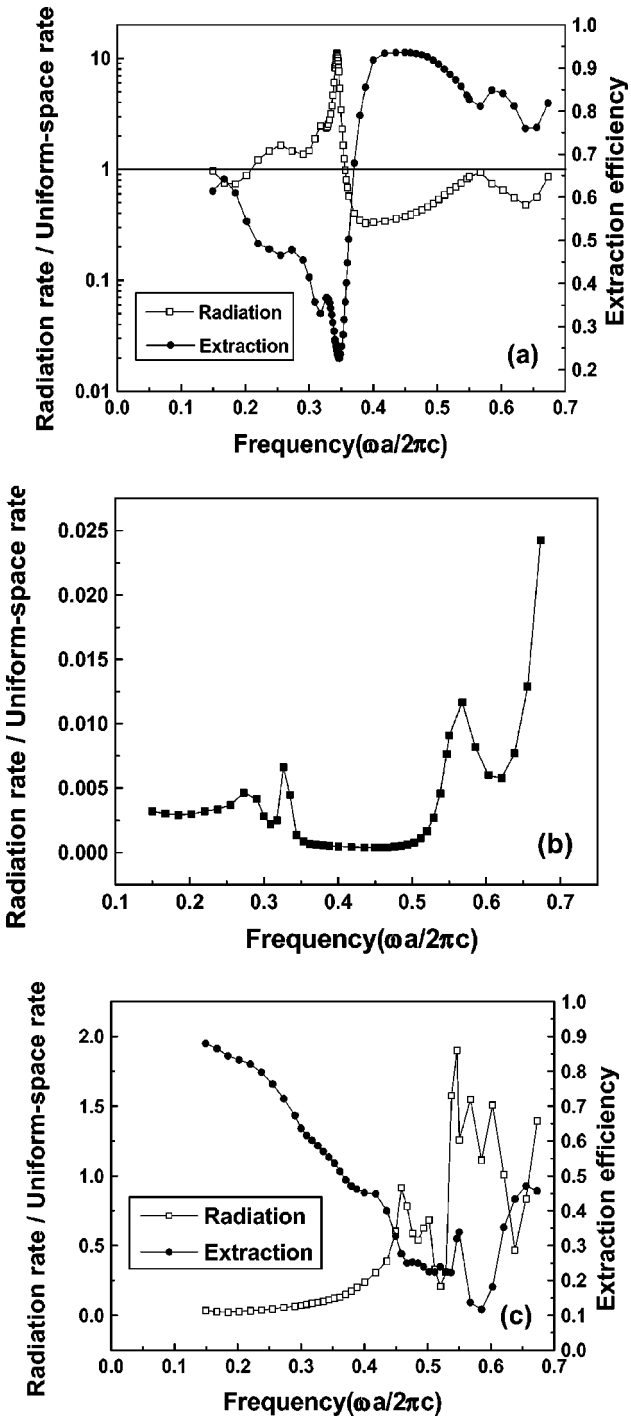

FIG. 6. Radiation rate of a dipole at the center of the structure shown in Fig. 5 (a) relative to the rate in uniform space ($\epsilon_s = 12.25\epsilon_o$). (a) An E_y-polarized point dipole with output efficiency along the z direction. (b) An E_x-polarized point dipole. (c) An E_z-polarized point dipole with output efficiency along the z direction.

The radiation rate and the extraction efficiency for an E_y-polarized point dipole at the center of the slab is shown in Fig. 6(a). The radiation rate is enhanced near the band edge of the lowest band and reduced inside the TE-like band gap, while the extraction efficiency is small near the band edge composed of the guided modes and large inside the TE-like band gap. The radiation rate for an E_x-polarized point dipole is shown in Fig. 6(b). The radiation rate is small compared to

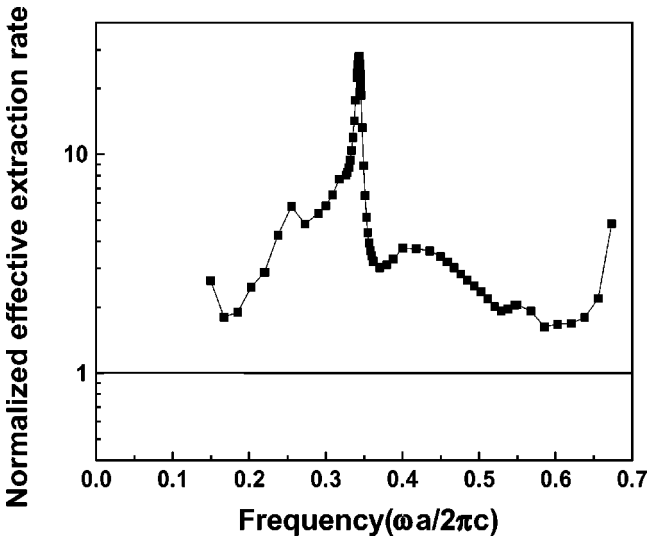

FIG. 7. The effective extraction rate for an E_y-polarized point dipole normalized to that of the uniform slab.

that of an E_y-polarized point dipole. It is due to the low coupling at that position. The radiation rate is proportional to the square of the amplitude of the electric field. The radiation rate for an E_z-polarized point dipole is shown in Fig. 6(c). A localized mode is introduced in the TM-like band gap compared to the photonic band diagram in Fig. 5(b). In the real experiment, the multiplication of the radiation rate and the extraction efficiency is related to the measured light emitted from the slab, depending on the excitation and measuring scheme. We define this multiplication as the effective extraction rate from now on. In Fig. 7, we draw the effective extraction rate for the etched slab normalized to that of the uniform slab for an E_y-polarized point dipole. The spatial dependence of the radiation rate is not included in this figure. However, for the most frequencies, the effective extraction rate for the etched slab is larger than that of the uniform slab for a point dipole located at the center. Especially, the effective extraction rate is largest near the band edge. Here the low extraction efficiency is overcome by the larger enhancement of the radiation rate. However, this does not necessarily mean the band-edge region is better for light-emitting diodes. In this frequency region more light is guided inside the slab.

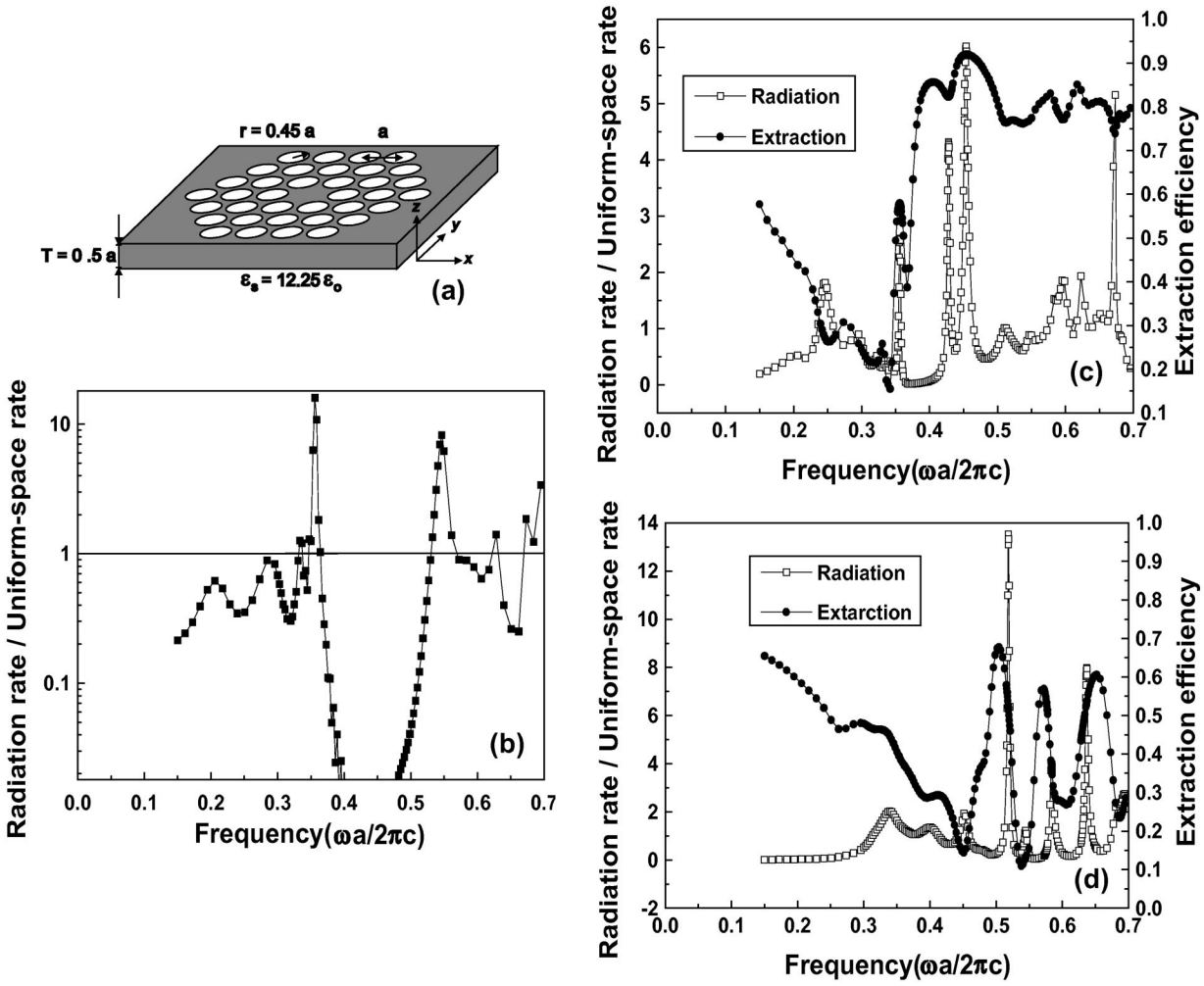

FIG. 8. (a) Schematic diagram of the computational cell containing a cavity based on a dielectric slab with air holes on a triangular lattice. (b) Radiation rate of an E_y-polarized point dipole at the center of the structure relative to the rate in uniform space ($\epsilon_s = 12.25\epsilon_o$). (c) An E_y-polarized point dipole at $0.45a$ shifted along the x axis from the center of the structure. (d) An E_z-polarized point dipole at the center of the structure relative to the rate with output efficiency along the z direction.

E. Finite triangular lattice slab with a defect

The triangular slab with defects[10] is more interesting because it has the potential for a low threshold laser or a light-emitting diode with the high extraction efficiency and the enhanced spontaneous emission rate. The radiation rate in the triangular slab with a defect as in Fig. 8(a) is shown in Fig. 8(b). With an E_y-polarized point dipole located in the center of the defect, the inhibition of the radiation rate is found in the TE-like band gap and the enhancement of the radiation rate near the band edge is observed. However, the emission related to the localized defect mode is not noticeable in the TE-like band gap. This can be explained by the fact that electric-field distributions for the defect modes have very small amplitudes at the center of the defect.[6] To verify this overlap factor, the position of the E_y-polarized point dipole is shifted to $0.45a$ along the x axis. As shown in Fig. 8(c), several emission lines associated with defect modes are observed inside the TE-like band gap. The radiation rates are enhanced at the defect-mode frequencies. The extraction efficiencies are also high at the defect-mode frequencies. The result for an E_x-polarized point dipole also shows similar behavior. For an E_z-polarized point dipole, the defect modes were found in the TM-like band gap as shown in Fig. 8(d).

The effective extraction rate for the shifted E_y-polarized point dipole is shown in Fig. 9. The results are normalized to those of the uniform slab for the same polarization. One can see that the effective extraction rates are large at the defect-mode frequencies compared to those of the uniform slab. This result is attributed to the enhanced spontaneous emission and the high extraction efficiency. These characteristics are important to light-emitting diodes. Further studies are needed to extend these results to the case of stimulated emission.

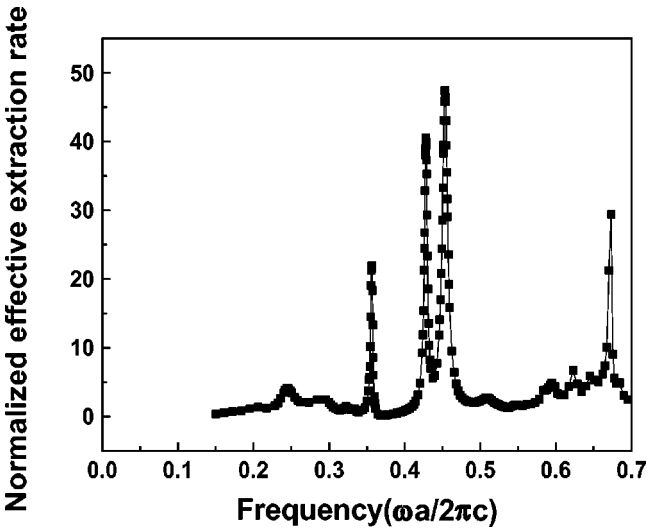

FIG. 9. The effective extraction rate for an E_y-polarized point dipole normalized to that of the uniform slab. The position of the dipole is shifted from the center of the defect to $0.45a$ along the x axis.

IV. CONCLUSION

The spontaneous emission rate of a dipole in the microcavity is calculated by directly solving the inhomogeneous Maxwell's equation in real space with the finite-difference time-domain method to deal with general geometries and frequency distributions. The spontaneous emission which is the summation of the radiation rate to all the allowed modes is obtained all at once without summing the radiation rate of each mode. This approach dose not need the field distributions of the allowed modes and dispersion relation. Localized modes, guided modes, and extended modes are inherently included. The agreement between this approach and analytic solutions in a planar cavity was good for a continuum of resonance modes. For photonic band-gap structures, the frequency regions of the inhibition and enhancement of the spontaneous emission agree well relative to the photonic band diagram. A comparison between the line dipole and the point dipole is made for the square lattice, where the effects of an off-plane propagation in the in-plane band gap on the radiation rate are shown in a continuum with localized states. In a triangular slab with and without a defect, the spontaneous emission rates are calculated. The triangular slab with a defect shows the enhanced spontaneous emission rate and the high extraction efficiency at the defect-mode frequencies compared with those of the uniform slab.

Quite recently, the method of calculating the spontaneous emission lifetimes of the dipole was independently developed and applied to a slab waveguide and a dielectric microdisk by another group with the use of the finite-difference time-domain method.[36]

ACKNOWLEDGMENTS

We thank A. Scherer for useful discussions. This work was supported by the research project for basic science of the Korea Advanced Institute of Science and Technology.

[1] E. M. Purcell, Phys. Rev. **69**, 681 (1946).
[2] D. Kleppner, Phys. Rev. Lett. **47**, 233 (1981).
[3] E. A. Hinds, in *Cavity Quantum Electrodynamics*, edited by P. R. Berman (Academic Press, Inc, Orlando, 1994).
[4] E. Yablonovitch, Phys. Rev. Lett. **58**, 2059 (1987).
[5] S. John, Phys. Rev. Lett. **58**, 2486 (1987).
[6] J. D. Joannopoulos, R. D. Meade, and J. N. Winn, *Photonic Crystal* (Princeton University Press, Princeton, 1995).
[7] J. D. Joannopoulos, P. R. Villeneuve, and S. Fan, Solid State Commun. **102**, 165 (1997).
[8] H. Yokoyama, Science **256**, 66 (1992).
[9] S. Fan, P. R. Villeneuve, J. D. Joannopoulos, and E. F. Schubert, Phys. Rev. Lett. **78**, 3294 (1997).
[10] M. Boroditsky and E. Yablonovitch (unpublished).
[11] G. S. Agarwal, Phys. Rev. A **12**, 1475 (1975).
[12] J. P. Dowling, Found. Phys. **23**, 895 (1993).
[13] T. Baba, T. Hamano, F. Koyama, and K. Iga, IEEE J. Quantum Electron. **27**, 1347 (1991).
[14] T. Baba and M. Koma, Jpn. J. Appl. Phys., Part 1 **34**, 1405 (1995).
[15] J. P. Dowling and C. M. Bowden, Phys. Rev. A **46**, 612 (1992).
[16] K. Sakoda and K. Ohtaka, Phys. Rev. B **54**, 5732 (1996).

[17] T. Suzuki and P. K. L. Yu, J. Opt. Soc. Am. B **12**, 570 (1995).
[18] K. Sakoda and H. Shiroma, Phys. Rev. B **56**, 4830 (1997).
[19] K. Sakoda, J. Appl. Phys. **84**, 1210 (1998).
[20] K. Sakoda, T. Ueta, and K. Ohtaka, Phys. Rev. B **56**, 14 905 (1997).
[21] K. S. Lee, IEEE Trans. Antennas Propag. **AP-14**, 302 (1966).
[22] J. P. Berenger, J. Comput. Phys. **114**, 185 (1994).
[23] C. E. Reuter, R. M. Joseph, E. T. Thiele, D. S. Katz, and A. Taflove, IEEE Microwave Guid. Wave Lett. **4**, 344 (1994).
[24] C. M. Furse and O. P. Gandhi, IEEE Microwave Guid. Wave Lett. **5**, 326 (1995).
[25] W. Jhe, A. Anderson, E. A. Hinds, D. Meschede, L. Moi, and S. Haroche, Phys. Rev. Lett. **58**, 666 (1987).
[26] K. L. Shlager, J. G. Maloney, S. L. Ray, and A. F. Peterson, IEEE Trans. Antennas Propag. **AP-41**, 1732 (1993).
[27] J. P. Berenger, J. Comput. Phys. **127**, 363 (1996).
[28] P. R. Villeneuve, S. Fan, and J. D. Joannopoulos, Phys. Rev. B **54**, 7837 (1996).
[29] R. D. Meade, K. D. Brommer, A. M. Rappe, and J. D. Joannopoulos, Appl. Phys. Lett. **61**, 495 (1992).
[30] A. A. Maradudin and A. R. McGurn, J. Mod. Opt. **41**, 275 (1994).
[31] X. P. Feng and Y. Arakawa, IEEE J. Quantum Electron. **32**, 535 (1996).
[32] M. M. Sigalas, R. Biswas, K. M. Ho, and C. M. Soukoulis, Phys. Rev. B **58**, 6791 (1998).
[33] R. D. Meade, A. M. Rappe, K. D. Brommer, and J. D. Joannopoulos, Phys. Rev. B **48**, 8434 (1993).
[34] S. Hyun, J. Hwang, Y. Lee, and S. Kim, Microwave Opt. Technol. Lett. **16**, 352 (1997).
[35] J. Hwang, S. Hyun, H. Ryu, and Y. Lee, J. Opt. Soc. Am. B **15**, 2316 (1998).
[36] Y. Xu, J. S. Vučković, R. K. Lee, O. J. Painter, A. Scherer, and A. Yariv, J. Opt. Soc. Am. B **16**, 465 (1999).